CISTER
Research Centre in
Real-Time & Embedded
Computing Systems

Conference Paper

On the Performance of an Air-Water Visible Light Communication System

Guillermo Martínez
Pablo Palacios Játiva
Miguel Gutiérrez Gaitán*
Cesar A. Azurdia Meza
Nicolás Boettcher
David Zabala Blanco

*CISTER Research Centre

CISTER-TR-240802

2024/10/21

On the Performance of an Air-Water Visible Light Communication System

Guillermo Martínez, Pablo Palacios Játiva, Miguel Gutiérrez Gaitán*, Cesar A. Azurdia Meza, Nicolás Boettcher, David Zabala Blanco

*CISTER Research Centre

Polytechnic Institute of Porto (ISEP P.Porto)

Rua Dr. António Bernardino de Almeida, 431

4200-072 Porto

Portugal

Tel.: +351.22.8340509, Fax: +351.22.8321159

E-mail: mjggt@isep.ipp.pt, nicolas.boettcher@mail.udp.cl, dzabala@ucm.cl

https://www.cister-labs.pt

Abstract

Research on wireless communication in water environments is gaining attention due to its relevance in enabling and supporting new applications under the Underwater Internet of Things (UIoT) umbrella. Visible Light Communication (VLC) is one of the emerging communication technologies with the potential to contribute to this domain, especially concerning direct communications from above the surface to underwater nodes. Although more traditional radio frequency (RF) communications are not suitable for air-to-water communications, VLC offers unique opportunities in this area. In this respect, this work presents a simulative study attempting to theoretically understand the performance of VLC systems in both underwater and air-to-water channels. We explore performance metrics including, link gain, time delay, and bit-error rate, while analyzing the optical signal interruption on the sea surface due to water level changes. The investigation offers preliminary results that shed light on the feasibility and challenges of effectively enablingcross-border air-water communication systems using VLC technologies.

© 2024 CISTER Research Center
www.cister-labs.pt

On the Performance of an Air-Water Visible Light Communication System

Guillermo Martínez[1], Pablo Palacios Játiva[1], Miguel Gutiérrez Gaitán[23], César Azurdia Meza[4], Nicolás Boettcher[1], and David Zabala-Blanco[5]

[1] Universidad Diego Portales, Chile
{guillermo.martinez,pablo.palacios,nicolas.boettcher}@mail.udp.cl
[2] Pontificia Universidad Católica de Chile, Chile
{miguel.gutierrez}@uc.cl
[3] CISTER Research Centre, Porto, Portugal
{mjggt}@isep.pt
[4] Universidad de Chile, Chile
{cazurdia}@ing.uchile.cl
[5] Universidad Católica del Maule, Chile
{dzabala}@ucm.cl

Abstract. Research on wireless communication in water environments is gaining attention due to its relevance in enabling and supporting new applications under the Underwater Internet of Things (UIoT) umbrella. Visible Light Communication (VLC) is one of the emerging communication technologies with the potential to contribute to this domain, especially concerning direct communications from above the surface to underwater nodes. Although more traditional radio frequency (RF) communications are not suitable for air-to-water communications, VLC offers unique opportunities in this area. In this respect, this work presents a simulative study attempting to theoretically understand the performance of VLC systems in both underwater and air-to-water channels. We explore performance metrics including, link gain, time delay, and bit-error rate, while analyzing the optical signal interruption on the sea surface due to water level changes. The investigation offers preliminary results that shed light on the feasibility and challenges of effectively enabling cross-border air-water communication systems using VLC technologies.

Keywords: Air-to-Water · VLC communication · Signal propagation.

1 Introduction

Optical wireless communication across the boundary between air and water has gained significance because of its capability to allow efficient, high-speed data transfer between nodes located underwater and stations on land or in the air. [1]. Although various alternatives have been explored in the literature, such as radio-frequency (RF) communication and magnetic-induction (MI) communication [2], none have demonstrated satisfactory performance for cross-border air-water communication. RF communication, while effective for *overwater* transmission under certain distance and height configurations [3, 4], suffers from high attenuation *underwater* due to the skin effect, significantly limiting its applicability. Similarly, although MI methods provide Doppler-effect-free communication, their range is known to be restricted by the conductivity of water.

Despite these hurdles, air-water communication research has seen notable advancement in recent years, driven by the need to help various maritime applications such as underwater exploration, monitoring of marine pollution, and military activities [5]. This increased focus on air-water communication has led to an intensive search for innovative and robust solutions capable of overcoming the inherent obstacles associated with transmitting data across the water surface. Researchers and engineers are exploring a variety of advanced techniques and technologies to address challenges such as signal attenuation, reflection, refraction, and scattering at the air-water interface. These efforts aim to improve the reliability and efficiency of communication systems that need to operate seamlessly across this boundary. Innovations in modulation schemes, adaptive algorithms, and hybrid communication methods are being investigated to ensure that data can be transmitted with minimal loss and distortion. Furthermore, the development of specialized transceivers, optimized for the unique properties of air and water media, plays a crucial role in bridging the gap between these two environments [6]. Through these concerted efforts, significant progress is being made toward the achievement of effective and resilient air-water communication systems, which are essential for applications in oceanographic research, environmental monitoring, and maritime operations.

This research explores the main elements that impact the transmission of visible light communication (VLC) across the air-water boundary. The aim is to comprehend how VLC transmission is influenced by the unique dynamics and challenging environmental conditions of the water medium. For this purpose, we examine factors such as weather conditions, turbulence on the surface of the water, and optical signal scattering. In addition, we will explore methods to mitigate these challenges, focusing on air-water VLC communication efficiency and reliability. The overall study is motivated by the ability of light to efficiently traverse the air-water interface, which offers a reduced transmission time and faster propagation speed.

2 Related Works

Prior work has investigated air-water VLC communication, addressing various aspects of performance and reliability [1, 2]. Researchers have explored, for example, the impact of distinctive environmental factors such as water clarity, surface turbulence, and ambient light conditions on optical signal quality. Other studies have focused on optimizing transmitter and receiver designs to enhance signal strength and mitigate scattering and absorption effects. Error correction and adaptive modulation techniques have also been investigated to improve data integrity and transmission efficiency.

Despite the emerging and increasing interest of the research community in this area, several studies have already contributed to the understanding of the air-water channel. In the work in [7], the scintillation index (SI) is used to quantify the fluctuation of light intensity received in VLC communication. This helps in understanding the variability and stability of the communication link. The research in [8] discusses various communication parameters for evaluating the efficiency of direct VLC communication over the air-water interface. These parameters include data rate, communication distance, transceiver alignment, and stability under adverse environmental conditions. Similarly, the authors in [9] evaluate the efficiency of direct and relay-based VLC communication in cross-border air-water communication by studying parameters such as bit error rate (BER), data rate, communication distance, and coverage capability. A different work [9] highlights the importance of studying VLC communication efficiency in turbulence and power loss.

These studies collectively enhance our understanding of the variables influencing air-water VLC communication, guiding the development of more effective and resilient systems. Our work leverages the knowledge of the VLC air-to-water channel to address some of the challenges of cross-border communication while considering multiple parameters influencing performance. Moreover, as different from most existing literature, we focus particularly on water dynamics.

3 Air-Water VLC System Channel

This section presents the necessary background to analyze the VLC air-water channel. We present the transmission and reception elements, as well as the basic equations to describe the propagation of the signal in the air-water system considered.

3.1 VLC Air-Water Channel

Air-water communication in visible light systems involves navigating through three distinct environments, each of which significantly influences the communication channel: i) air, ii) water and iii) the air-water interface. Each of these environments presents unique characteristics and challenges that necessitate thorough analysis for a comprehensive understanding and practical implementation.

In the air environment, factors such as atmospheric conditions, air turbulence, and particle scattering must be considered, as they can affect the propagation of visible-light signals. The water environment, on the other hand, introduces challenges related to absorption and scattering by water molecules and suspended particles, which can greatly diminish the intensity and clarity of the transmitted signal.

The air-water interface represents a particularly critical transition zone where light signals must cross from one medium to another, encountering phenomena such as refraction, reflection, and potential distortion. This interface can cause significant signal loss and alteration, making it an important factor in optimizing communication strategies.

Figure 1 provides a visual representation of this multi-environment scenario, highlighting the complexities and the need for tailored solutions to ensure efficient and reliable data transmission across these different mediums. By addressing the specific issues posed by each environment, researchers can develop more robust air-water communication systems that are capable of maintaining high performance despite the inherent challenges.

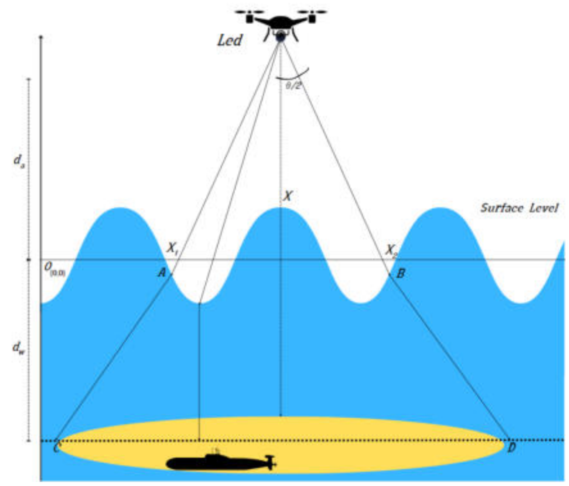

Fig. 1. Outline of the media/environments of a VLC Air-Water system.

Air Channel The air is the first transmission medium in the integrated VLC air-water channel. The light emitted by light-emitting diodes (LEDs) propagates through the air to transmit the data. Air, as a transmission medium, has a constant light propagation speed, but its optical properties can significantly affect the communication quality. Light signal attenuation must be carefully managed due to scattering, reflection, and absorption in airborne particles such as dust or water droplets. In addition, physical obstacles in the air can cause reflections and light scattering, generating shadows and areas of interference [10, 11].

Water Channel The water channel is the transmission medium when VLC communication extends to water, such as underwater applications. Unlike air, water has different optical properties. The speed of light propagating through water is roughly 1.33 times less than that of air, indicating altered signal travel time and an increased likelihood of scattering. The weakening of the signal in water is more pronounced as a result of absorption and scattering of light in water molecules and suspended particles. VLC communication in water is applicable in aquatic environments, such as swimming pools, tanks, or marine applications, where data transmission is achieved by propagating light through water.

Air-Water Transition The transition between the air and water channels represents a critical challenge in VLC communication between air and water. The interface between these two media introduces changes in the light path due to refraction, which can result in signal loss and the need to adjust the orientation of the transmitters and receivers to ensure a smooth transition and uninterrupted communication.

3.2 Transmission and Reception Elements

In Air-Water VLC systems, several components are used for both transmitting and receiving data. Transmitters include LEDs and laser diodes (LDs), while receivers can be P-N Junction Photovoltaic Diodes (PIN), Avalanche Photovoltaic Diodes (APDs), Silicon Photomultipliers (SiPMs) and Multi-Pixel Photon Counters (MPPCs).

Each of these components has specific characteristics that affect the quality and efficiency of communication in air-to-water environments. The proper choice of these components, their arrangement and calibration are critical to ensure robust and reliable data transmission in this context.

4 Propagation model in VLC Air-Water systems

The basic point to consider is that the surface of the water rarely appears as a flat surface and is usually characterized by the presence of waves due to the action of the wind. Therefore, modeling this feature with an exact mathematical expression that describes these surface waves is challenging, as they depend mainly on the depth of the water and the wind speed. This characterization can be seen in Figure 2.

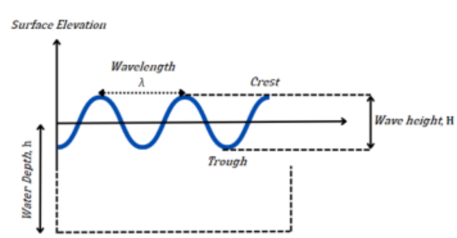

Fig. 2. Illustration of the shape of a cnoidal wave.

This characterization is well defined, based on the expression that is called the cnoidal wave equation:

$$\eta(x,t) = \eta_2 + H \cdot J_2\left(\frac{x - c \cdot t}{\varDelta}|m\right), \tag{1}$$

The notation η denotes the surface elevation, x stands for the horizontal position, t refers to time, H is the height of the wave, η_2 signifies the elevation of the trough, c is the speed of the phase, and J represents one of the Jacobi elliptic functions. Consequently, η_2, $\varDelta$, λ, and c can be defined as:

$$\eta_2 = \left(\frac{H}{m}1 - m - \frac{E(m)}{K(m)}\right), \left(\varDelta = \frac{\lambda}{2K(m)} = h\sqrt{\frac{4mh}{3H}}\right), \tag{2}$$

$$c = \sqrt{gh}\left[1 + \frac{H}{mh}\left(1 - \frac{1}{2}m - \frac{3E(m)}{3K(m)}\right)\right], \tag{3}$$

$$\tau = \frac{\lambda}{c}. \tag{4}$$

Alternatively, the propagation of waves, described by Stokes wave theory, is relevant to both intermediate and deep water [12]. Deep water is defined when the water depth significantly exceeds the wavelength ($h > \lambda$). Based on Stokes' third-order theory, the height of the water surface can be represented as follows:

$$H = 2\alpha\left(1 + \frac{3}{8}(k\alpha)^2\right), \tag{5}$$

where $(k\alpha)$ is the steepness of the wave.

This research explores the application of a light source for transmitting signals across the interface between air and water. In our approach, a light source is placed at a determined altitude above the water and aimed downward. Subsequently, the light intensity is measured at different underwater depths. We employed a light source with an adjustable beam angle, enabling us to regulate both the intensity and the dispersion area of the light within the water. A summary of the parameters used in this work is shown in Table 1.

Figure 3 presents a three-dimensional view of an individual light transmitter S and its resulting underwater coverage area. To determine the limits of the coverage area, we begin with a cross-section of a cone, specifically the 2D plane generated by the two light beams SA and SB on the cone's surface, and then pinpoint the corresponding underwater points C and D at this boundary. By rotating this plane, two more boundary points can be established. By continuously rotating the plane through 360°, we can completely outline the underwater coverage area, as explained below.

Figure 4 presents a detailed illustration of the 2D plane used in the initial step. The x-axis of Figure 4 represents the level of water without the presence of waves; from this, the surface of the water extends and becomes wavy. The point $O_{(0,0)}$ is regarded as the origin. A light source is situated at the point $S(x_s, y_s)$, positioned at a distance d_a above the water surface. θ denotes the beam angle of the light source. The beam SE originates from the light source S and strikes the

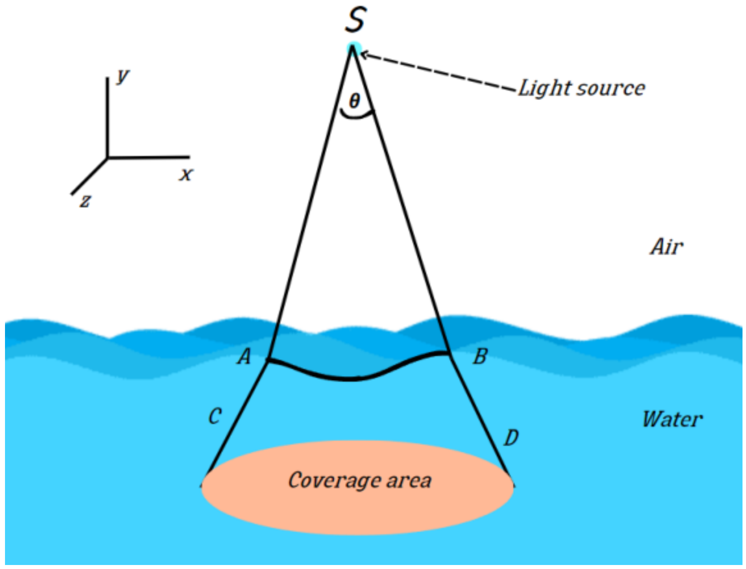

Fig. 3. 3D view of an in-water coverage area.

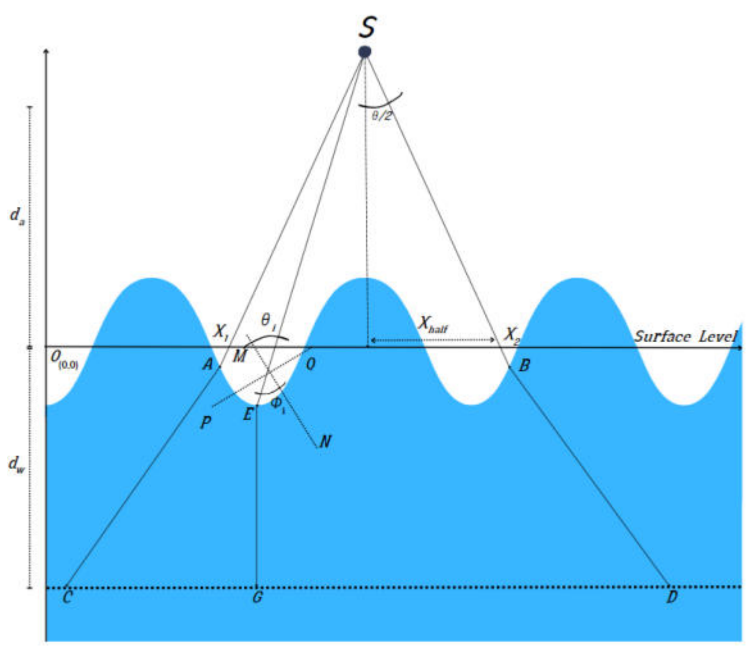

Fig. 4. Illustration of the direction of light rays on a wavy surface.

water surface at the point $E(x_e, y_e)$ with an incident angle θ_i relative to the MN line. The light ray changes direction at the point $G(x_g, y_g)$, originating from the point E, forming a transmission angle ϕ_i.

Now, we assume that the water surface is described by the function:

$$y = f(x). \tag{6}$$

For a fluctuating water surface, the surface function can be derived using either Eq. (1) or Eq. (4). Conversely, for a level surface, it is merely a straight line. The first derivative of the surface function at any given point on the water surface represents the tangent at that point. Consequently, the slope at point E is:

$$m_{PQ} = f'(x_e). \tag{7}$$

To determine the incident angle θ_i, it is necessary to find the slopes of SE and MN, which are given by:

$$m_{SE} = \frac{y_s - y_e}{x_s - x_e} = \frac{y_s - f(x_e)}{x_s - x_e}, \tag{8}$$

$$m_{MN} = \frac{-1}{m_{PQ}} = \frac{-1}{f'(x_e)}. \tag{9}$$

At this moment, the angle between SE and MN measures:

$$\theta_i = \tan^{-1}\left|\frac{f'(x_e)(y_s - f(x_e)) + (x_s - x_e)}{(x_s - x_e)f'(x_e) - y_s + f(x_e)}\right|. \tag{10}$$

Given the incident angle, θ_i, we can determine the transmission angle ϕ_i using Snell's law:

$$\eta_a \cdot \sin(\theta_i) = \eta_w \cdot \sin(\phi_i). \tag{11}$$

Therefore, the slope of the EG line is as follows:

$$m_{EG} = \frac{y_g - f(x_e)}{x_g - x_e} \rightarrow x_g = x_e + \frac{y_g - f(x_e)}{m_{EG}}. \tag{12}$$

Table 1. Important notations throughout the article.

Notation	Description
θ	Angle of the light beam's source
θi	Angle at which light hits the surface of the water
ϕ	Angle at the boundary of the refracted light beam
ϕi	Angle of refraction for the light beam
d_w	Depth at which the node is located underwater
d	Diameter of the coverage area
d_a	Distance between the light source and the surface
P	Power of single light source
η	Reflection of light
τ	Transmission of light

Now the relationship between ϕ_i , m_{EG} y m_{MN} is:

$$\tan(\phi_i) = \left| \frac{m_{MN} - m_{EG}}{1 + m_{MN} \cdot m_{EG}} \right| . \tag{13}$$

If we expand the expression (14) for m_{EG} then we get:

$$\begin{aligned} (m_{MN}^2 \cdot \tan(\phi_i^2) - 1) \cdot m_{EG}^2 + 2 \cdot m_{MN} \cdot (1 + \tan(\phi_i^2)) \cdot m_{EG} + \\ \tan(\phi_i^2) - m_{MN}^2 = 0. \end{aligned} \tag{14}$$

4.1 Convergence Area

Given the preceding analysis, for a specified function and the light source's location, we can determine the refracted ray in water at a specified surface point. Figure 4 illustrates a straightforward scenario where SA and SB are the boundary rays in the air, while AC and BD are the corresponding refracted rays. Therefore, knowing points A and B allows us to ascertain points C and D, with line CD representing all points through which the refracted ray travels post-refraction. Figure 4 depicts X_1 and X_2 as the points where the SA and SB lines intersect the x-axis. For a given angle θ, the distance from the midpoint of the segment $X_1 X_2$ to either X_1 or X_2 is determined by the follow expression:

$$X_{half} = d_a \tan(\frac{\theta}{2}). \tag{15}$$

At this point, we can readily determine the coordinates of X_1 and X_2 as:

$$X_1 \equiv (X_s - X_{half}, 0), \tag{16}$$

$$X_2 \equiv (X_s + X_{half}, 0). \tag{17}$$

The equation for line SX_1 (or SA) is:

$$\begin{aligned} \frac{x - x_S}{x_S - x_S + X_{half}} &= \frac{y - y_s}{y_S - 0}, \\ \rightarrow \; y_S \cdot x - X_{half} \cdot y - x_S \cdot y_S + X_{half} \cdot y_S &= 0. \end{aligned} \tag{18}$$

4.2 Modeling of power received

Water The key optical properties of the underwater medium that significantly impact the transmission of light are the absorption and scattering coefficients. The absorption coefficient quantifies the rate at which optical photons are absorbed by water and its constituents, such as dissolved organic matter, phytoplankton, and various other particulates. This absorption process converts the energy of the optical photons into other forms, primarily heat, thereby diminishing the intensity of the light signal as it penetrates deeper into the water. On the other hand, the scattering effect can occur in all directions and is influenced by factors such as the size, shape, and refractive index of the particles. This deflection causes the light signal to spread out and lose its directivity, making it more difficult to maintain a clear and coherent signal over longer distances.

Together, the absorption and scattering coefficients define the attenuation of light in the underwater environment, which is the combined effect of the reduction in signal intensity and the dispersion of light. The attenuation coefficient, represented as C(λ), is typically utilized to describe how light propagates in water. This coefficient is the aggregation of the absorption and scattering coefficients. Therefore, C(λ) is expressed as follows:

$$C(\lambda) = a(\lambda) + b(\lambda). \tag{19}$$

In this context, the coefficients a(λ) and b(λ) are influenced both by the type of water and the wavelength λ. Simplifying the modeling of various water types can be achieved by adjusting the chlorophyll C concentration. Consequently, the coefficients a(λ) and b(λ) can be represented as:

$$a(\lambda) = [a_w(\lambda) + 0,06 a_c(\lambda) C^{0,65}] \cdot [1 + 0,2^{-0,014(\lambda - 449)}], \tag{20}$$

$$b(\lambda) = 0,30 \cdot \frac{550}{\lambda} \cdot C^{0,65}, \tag{21}$$

where a_w denotes the absorption coefficient of pure water, and a_c stands for the specific absorption coefficient of chlorophyll, which is a dimensionless value derived through statistical analysis.

Table 2 summarizes the measured values for the aforementioned coefficients for four types of seawater. The type of water selected in this work is clean seawater.

Table 2. Table of values according to type of water.

Water types	C(mg/m^3)	a(λ) (m^{-1})	b(λ) (m^{-1})	c(λ) (m^{-1})
Pure Water	0,005	0,53	0,003	0,056
Clean Water	0,31	0,069	0,08	0,151
Coast Water	0,83	0,088	0,216	0,305
Turbid Water	5,9	0,295	1,875	2,170

As light travels a particular distance z, the overall power attenuation can be described using the Beer-Lambert law. This is represented by:

$$I(\lambda, z) = I_0^{-c(\lambda)\cdot z}, \tag{22}$$

with I_0 representing the irradiance at the source and I denoting the irradiance at the receiving end.

Air Optical signals propagating through the atmosphere can experience significant attenuation due to various factors, including the presence of molecular constituents such as water vapor, carbon dioxide, and other gases, as well as aerosols like dust, smoke, and pollution particles [13]. This attenuation is primarily caused by two mechanisms: absorption and scattering. Absorption occurs when the energy of the optical signal is absorbed by the atmospheric molecules and aerosols, converting it into other forms of energy, such as heat. Scattering, on the other hand, occurs when the path of the optical signal is redirected by these particles, causing the signal to spread out and lose intensity. As a result, accurately measuring and modeling the attenuation coefficient is essential for optimizing the reliability and efficiency of optical systems operating in atmospheric environments. Therefore, this relationship can be expressed as:

$$C(\lambda) = \alpha_m(\lambda) + \alpha_a(\lambda) + \beta_m(\lambda) + \beta_a(\lambda). \tag{23}$$

Here, $\alpha_m(\lambda)$ and $\alpha_a(\lambda)$ denote the molecular and aerosol absorption coefficients, while $\beta_m(\lambda)$ and $\beta_a(\lambda)$ represent the scattering coefficients for molecules and aerosols, respectively. Absorption varies selectively with wavelength. To align with atmospheric transmission windows, the wavelengths are specifically chosen, leading to scattering becoming the predominant factor in the attenuation coefficient. Consequently, the attenuation is mainly reduced to $\beta_a(\lambda)$. Empirical formulas are available to describe the scattering-induced attenuation, as given by:

$$\beta_a(\lambda) = \frac{3,91}{V}(\frac{\lambda}{550})^{-\delta}, \tag{24}$$

where V represents the visibility range in kilometers, defined as the distance that a light beam can travel through the atmosphere until its intensity drops to 5% of its original value and δ can be obtained based on Kruse's model [14].

4.3 Analysis and Results

In Figure 6, we can observe a 2D representation of how the convergence area is bounded by two light rays that are identified as the trace of AD and BC, The convergence area is understood as the distance between CD. Continuing with the above, it can be seen that Figure 5 represents the function that simulates the 3D water surface. The objective of the test is to see how the power of a beam of light behaves against the constant movement of water, and also to see how the type of water in which it is found affects the power underwater. Due to the great complexity of the simulation of water movement, it was decided to use a sine wave, which will simulate the water surface, and to simulate the movement of this, only proceeded to dephase in each iteration, obtaining as a general result a function very similar to the one that simulates the water surface, only inversely proportional, this means that when the water power is higher is because the water surface is at a lower level, otherwise, when there is less power, it is because the water surface is at its highest point, as can be seen in Figure

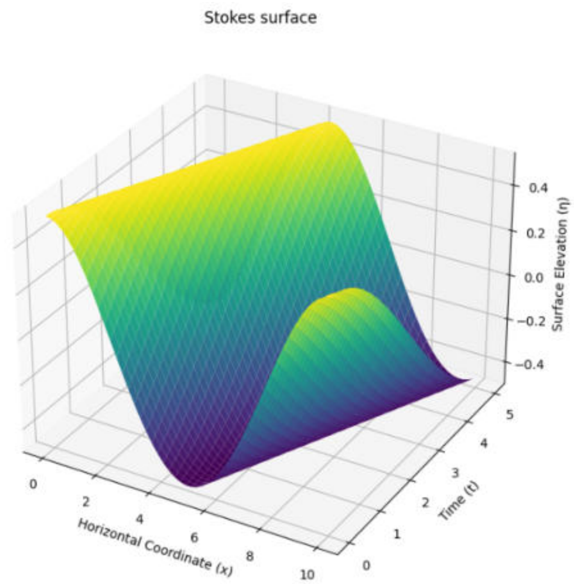

Fig. 5. Deep waters

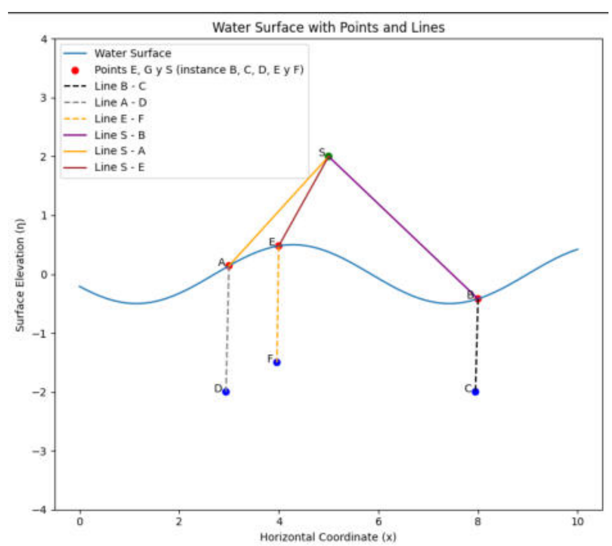

Fig. 6. Simulation of deep water surface

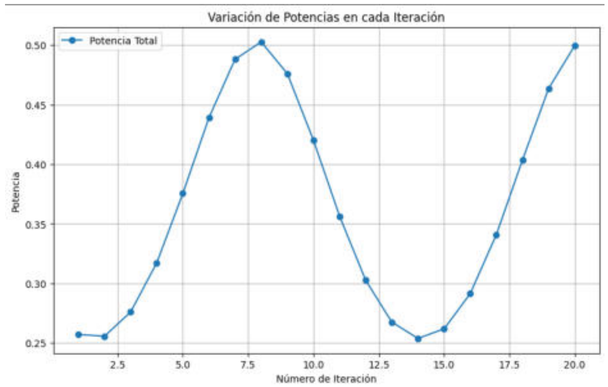

Fig. 7. shallow waters

7. Once the behavior of the power data shown in the graph was understood, we proceeded to measure this instance for each type of water mentioned above, this means that, in each type of water, 20 times were introduced to simulate that the water surface moves. As can be seen in Figure 8, the difference is obvious at the time of making the power calculations for each type of water, having as the best candidates clean water and coastal water, followed by pure water, leaving as the worst medium for the passage of light the turbid coastal water.

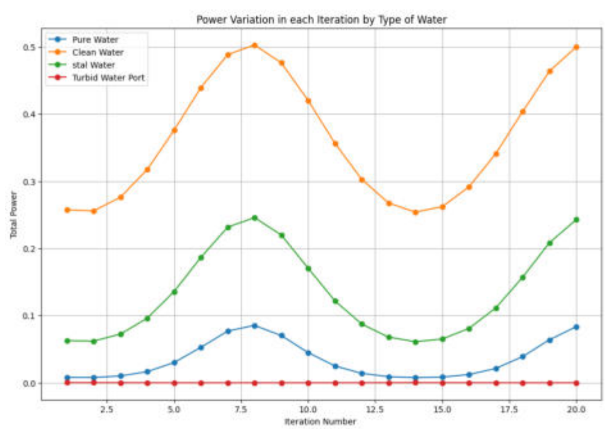

Fig. 8. Deep water power

5 Conclusions

The detailed research and analysis presented in this study on wireless optical air-to-water communication (VLC) has revealed a number of significant findings. Through mathematical modeling and simulation, a thorough understanding of the various factors that influence the efficiency and quality of communication in air-to-water environments has been achieved, providing valuable insights for the design and implementation of VLC communication systems in such challenging scenarios.

It has been shown that the transition between the air channel and the water channel represents a critical challenge in VLC communication, and changes in the light path due to refraction have been identified as a key factor affecting signal loss and the need to adjust the orientation of transmitters and receivers. In addition, a detailed approach to determine the effective coverage in water has been provided, considering light cone propagation and refraction at the air-water interface, providing a more accurate understanding of the light intensity distribution in aquatic environments.

Regarding the received power model, the importance of considering the absorption and scattering coefficients in both air and water has been highlighted, allowing an accurate evaluation of the signal attenuation along the optical propagation in these media. The results obtained from the simulation show how these factors affect the strength of the received signal and provide valuable information on how to optimize the parameters of the system to improve communication efficiency.

This study has shed light on the challenges and opportunities associated with VLC communication in air-water environments, providing a solid framework for future research and the development of robust and reliable communication systems for applications in this field. The findings could be extremely beneficial for engineers working on the design and deployment of optical communication networks in submarine and aquatic settings.

Acknowledgements This research was supported by FONDECYT Regular 1211132, FONDECYT Iniciación 11240799, FONDECYT Iniciación 11241221, ANID PFCHA/Beca de Doctorado Nacional/2019 (21190489), SENESCYT "Convocatoria abierta 2014-primera fase, (Acta CIBAE-023-2014)" and Escuela de Informática y Telecomunicaciones, Universidad Diego Portales; also by the CISTER Research Unit (UIDP/UIDB/04234/2020) through FCT/MCTES (Portuguese Foundation for Science and Technology) National Funds.

References

1. H. Luo, J. Wang, F. Bu, R. Ruby, K. Wu, and Z. Guo, "Recent progress of air/water cross-boundary communications for underwater sensor networks: A review," *IEEE Sensors Journal*, vol. 22, no. 9, pp. 8360–8382, 2022.

2. C.-C. Kao, Y.-S. Lin, G.-D. Wu, and C.-J. Huang, "A comprehensive study on the internet of underwater things: applications, challenges, and channel models," *Sensors*, vol. 17, no. 7, p. 1477, 2017.
3. M. G. Gaitán, P. M. Santos, L. R. Pinto, and L. Almeida, "Experimental evaluation of the two-ray model for near-shore wifi-based network systems design," in *IEEE 91st Vehicular Technology Conference (VTC2020-Spring)*. IEEE, 2020, pp. 1–3.
4. ——, "Optimal antenna-height design for improved capacity on over-water radio links affected by tides," in *Global OCEANS 2020: Singapore–US Gulf Coast*. IEEE, 2020, pp. 1–7.
5. M. F. Ali, D. N. K. Jayakody, Y. A. Chursin, S. Affes, and S. Dmitry, "Recent advances and future directions on underwater wireless communications," *Archives of Computational Methods in Engineering*, vol. 27, pp. 1379–1412, 2020.
6. F. K. Banaseka, F. Katsriku, J. D. Abdulai, K. S. Adu-Manu, and F. N. A. Engmann, "Signal propagation models in soil medium for the study of wireless underground sensor networks: A review of current trends," *Wireless Communications and Mobile Computing*, vol. 2021, no. 1, p. 8836426, 2021.
7. W. Aman, S. Al-Kuwari, M. Muzzammil, M. M. U. Rahman, and A. Kumar, "Security of underwater and air–water wireless communication: State-of-the-art, challenges and outlook," *Ad Hoc Networks*, vol. 142, p. 103114, 2023.
8. L.-K. Chen, Y. Shao, and Y. Di, "Underwater and water-air optical wireless communication," *Journal of Lightwave Technology*, vol. 40, no. 5, pp. 1440–1452, 2022.
9. H. Luo, J. Wang, F. Bu, R. Ruby, K. Wu, and Z. Guo, "Recent progress of air/water cross-boundary communications for underwater sensor networks: A review," *IEEE Sensors Journal*, vol. 22, no. 9, pp. 8360–8382, 2022.
10. P. P. Játiva, C. A. Azurdia-Meza, I. Sánchez, F. Seguel, D. Zabala-Blanco, A. D. Firoozabadi, C. A. Gutiérrez, and I. Soto, "A vlc channel model for underground mining environments with scattering and shadowing," *IEEE Access*, vol. 8, pp. 185 445–185 464, 2020.
11. P. P. Játiva, I. Soto, C. A. Azurdia-Meza, I. Sánchez, R. Wang, and W. Kern, "Hybrid digital twin model for greenhouse and underground environments," *IEEE Access*, 2024.
12. M. Berti, A. Maspero, and P. Ventura, "Full description of benjamin-feir instability of stokes waves in deep water," *Inventiones mathematicae*, vol. 230, no. 2, pp. 651–711, 2022.
13. E. Alozie, A. Abdulkarim, I. Abdullahi, A. D. Usman, N. Faruk, I.-F. Y. Olayinka, K. S. Adewole, A. A. Oloyede, H. Chiroma, O. A. Sowande *et al.*, "A review on rain signal attenuation modeling, analysis and validation techniques: Advances, challenges and future direction," *Sustainability*, vol. 14, no. 18, p. 11744, 2022.
14. P. Corrigan, R. Martini, E. A. Whittaker, and C. Bethea, "Quantum cascade lasers and the kruse model in free space optical communication," *Optics Express*, vol. 17, no. 6, pp. 4355–4359, 2009.